Designing molecular nano-architectures on metals and on graphene

Gottardi, Stefano

Chapter 5

Self-assembly of molecules on graphene

This chapter discusses the adsortpion of organic molecules on graphene. The realization of molecular nano-architectures on graphene by self-assembly is a promising route towards novel electronic and opto-electronic devices. We focus our study on linear molecules having terminal cyano functionalities and compare the results to their behavior on coinage metal surfaces. The effect of thermal annealing and deposition of metal ad-atoms on the assembly was investigated. Templating effects are observed due to the substrate underneath the graphene layer. Moreover, modified chemical reactivity of the functional cyano groups for the formation of metal-coordination was found on graphene compared to pristine metal surfaces. The reactivity is found to depend on the substrate underneath the graphene due to the modification of graphene's doping and thus charge transfer with the molecular adsorbates. This is shown to have a strong impact on the final assembly. The realization of molecular honeycomb networks based on hydrogen-bonding was achieved with molecules featuring carboxylic groups. The possibility to open a band gap in graphene by quantum confinement of electrons was investigated. The work presented in this chapter was performed in collaboration with Juan Carlos Moreno-Lòpez, Jun Li, Leonid Solianyk, Leticia Monjas (molecules synthesis), Anna K. H. Hirsch, and Meike Stöhr.

5.1 Introduction

The functionalization of graphene with organic molecules has great potential for the development of novel organic electronics and opto-electronics. Electric, magnetic as well as optical properties of graphene can be manipulated by the addition of opportunely engineered molecules.[1,2] A very promising approach consists in the creation of highly-ordered molecular assemblies.[1,3–5] Nano-architectures featuring zero-, one- and two-dimensional structures could in principle be tailored on graphene by self-assembling molecular building blocks. Intermolecular interactions and molecule-substrate interactions are both critical in this process. The former can be tuned by the selection of specific functional end groups, while the latter is mainly related to the chemical reactivity and the potential landscape of the substrate. In this respect, one might think that self-assembly on graphene would differ from the case of a metal substrate mainly by a modified molecule-substrate interaction and with little influence on the molecule's functionality. However, the different interactions with the substrate lead to strong changes in the chemical reactivity of the functional molecular groups and subsequently, to modifications of the intermolecular interactions. For example upon adsorption of TCNQ and F_4TCNQ on graphene on Ruthenium(0001), a modification of the molecular states was shown resulting in the formation of either a close-packed assembly or isolated molecules due repulsive intermolecular interactions.[6] Thus, it is of utmost importance, for a deeper understanding and for future device applications, to study the relevant factors that influence self-assembly as well as the electronic and magnetic properties of individual molecules on graphene. Spin-lattices, topological insulators and superconductors are among the potential applications that might be achieved by an improved control over the self-organization of molecules on graphene.[7–9] In this respect, the realization of a highly-regular two-dimensional (2D) porous network of molecules on graphene is challenging. 2D porous networks of molecules can be readily prepared on metal surfaces as described in the previous chapters. However, it will be

shown that the same molecules on graphene, do not easily lead to the creation of non-trivial architectures. Indeed most of the reports in literature show indeed the formation of a simple close-packed assembly.[3,4,10] Only a few exceptions are present that are obtained at the liquid-solid interface.[11] The realization of non-trivial metal-coordinated molecular assembly structures on graphene has been predicted to lead to a new class of organic topological insulators.[7,8] For this reason, the quest for controlled nano-architectures on graphene is an appealing research challenge. Two-dimensional periodic superstructures, also called superlattices, are believed to lead to the opening of a band gap in graphene by symmetry breaking.[12] Moreover, such superlattices were shown to be able to tailor new dispersive bands by the quantum confinement of electrons of the surface state of Cu(111).[13] The possibility of quantum confinement of electrons in graphene by molecular superlattices is a very interesting possibility that is still lacking experimental evidence. In section 5.6, work in this direction is reported.

Opening of a band-gap in graphene is a fundamental step towards the realization of graphene-based organic transistors and sensors. For this reason, one of the main goals of this thesis work was to investigate nano-architectures on graphene with particular focus on the formation of highly-ordered 2D networks. At the same time, we aimed to obtain deeper insight into the fundamental parameters that govern the intermolecular as well as the graphene-molecule interactions. It will be shown in this chapter that the substrate underneath the graphene plays a role in the molecular self-assembly and, in particular, in the reactivity of the functional molecular groups. In this regard, molecules on graphene can behave quite differently than on highly ordered pyrolitic graphite (HOPG). While in general it can be said that graphene electronically decouples the molecules from the surface minimizing the hybridization of the molecular orbitals with the metal substrate, the substrate still plays a critical role in determining the charge transfer between graphene and the molecular species adsorbed.

We focus our study on the self-assembly of linear cyano-functionalized sexiphenyl (P6) and terphenyl (P3) molecules on epitaxial graphene on Cu(111). The modification of the assembly by the addition of different metal atoms (Au, Co, Ni and Fe) aimed at the realization of potentially interesting metal-organic frameworks is discussed in section 5.4. However, the addition of metal atoms did not result in the formation of networks typically observed on metal surfaces. A modified chemical reactivity of the cyano groups toward the formation of metal-coordination bonds is revealed and depends on the substrate underneath the graphene layer. We believe this behavior to be connected with the doping level of graphene that affects the molecule-graphene charge transfer. As a result, a modification of the self-assembly as well as the final electronic and magnetic properties of the formed nano-architecture should in general be expected. Finally, for comparison and completeness, we present the case of a 2D porous network on graphene based on hydrogen bonding. This is the case for 1,3,5-benzenetribenzoic acid (T4) and is reported in section 5.6. This system is a representative example to discuss the possibility of quantum confinement of electrons in graphene and the possibility of band gap opening by means of molecular networks.

5.2 Self-assembly of cyano-functionalized sexiphenyl molecules on graphene on Cu(111)

Graphene on Cu(111) is a weakly interacting system in comparison to epitaxial graphene grown on other transition metals;[14–17] the graphene layer is n-type doped by 380 meV. These extra electrons are (at least partially) transferred to the graphene from the surface state of Cu(111) that consequently shifts towards the Fermi energy by 170 meV (see Chapter 4). However, the weak coupling with the substrate makes graphene on Cu(111) a good playground for the study of molecular self-assembly. Gra-

phene on Cu(111) was prepared and characterized as shown in Chapter 4. P6 molecules were deposited on graphene on Cu(111) in UHV with the sample kept at room temperature. Prior to molecule deposition, thermal annealing of the graphene sample at about 520 K was performed. The thermal annealing is necessary to remove water and other volatile molecules that might adsorb on the graphene surface during the transfer of graphene through air. The molecules were sublimated from a Knudsen cell and the rate and coverage were calibrated with a quartz microbalance to have sub-monolayer coverages ($0.1 - 0.5$ ML) at a rate of about 0.2 Å/min. Figure 5.1 shows typical STM images of the self-assembly of P6 molecules on graphene acquired at 77 K. At sub-monolayer coverage, P6 molecules form large islands with a close-packed arrangement. The P6 islands nucleate mainly around graphene wrinkles. The Moiré pattern of graphene on Cu(111) is visible in the background and seems not to affect the assembly (Fig. 5.1A), in contrast to what was observed for example upon the adsorption of C_{60} on graphene on Ru(0001) where the valley regions of the Moiré were found to be favored adsorption sites.[1] These sites are created by the Moiré modulation of the potential landscape of graphene. In the case of metals that interact strongly with graphene, like Ru and Ni, the Moiré pattern induces both potential and topographic modulations in the graphene layer. In contrast, graphene on Cu(111) interacts weakly, thus, a less pronounced effect of the Moiré structure is expected. A closer inspection of the self-assembly reveals a side to side packing of the P6 molecules. This arrangement is very different compared with the behavior of P6 molecules on metals at low coverages (see for example on Au(111) in Chapter 3 or on Ag(111)[19,20]), but quite common for the case of long rod-like molecules on graphene[1] or HOPG.[21–23] The phenyl rings of the P6 molecules are imaged very clearly by STM revealing the presence of an alternating twisting of the phenyl rings. This points towards an electronic decoupling of the P6 molecules and (almost) no hybridization with the substrate. A decoupling effect of graphene was also reported in the case of other molecular systems

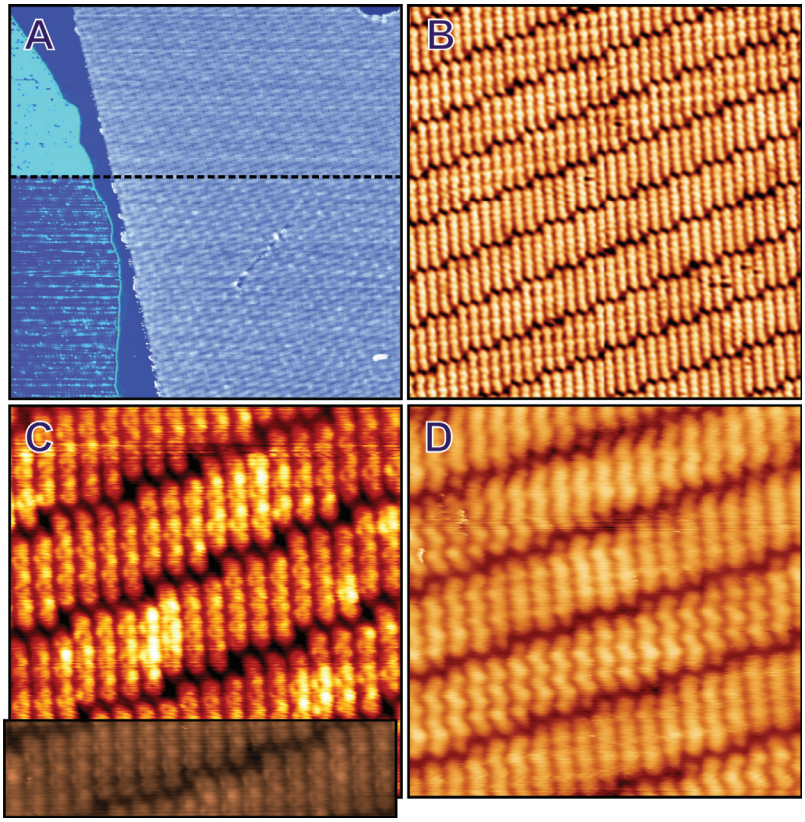

Figure 5.1: STM characterization of P6 molecules on graphene on Cu(111) at 77 K. **A)** Overview STM image (180 nm)^2, (V=−1.0 V, I=120 pA) showing an island of P6 molecules (on the right) that self-assembles in a close-packed phase. The Moiré pattern is visible as a modulation in the STM signal on the molecular island as well as on the pristine graphene (left side). The black dotted line marks a change of the tip termination. **B)** Detailed STM image (24 nm)^2, (V=−0.6 V, I=320 pA) of the P6 packing. Every 3 molecules a shift is present. **C)** High-resolution STM image (12 nm)^2, (V=−2.1 V, I=120 pA) showing sub-molecular features. The phenyl rings are visible displaying an alternating twisting of the phenyl rings. The inset shows a different color scale for comparison. **D)** STM image (12 nm)^2, (V=2.2 V, I=520 pA) acquired at positive bias. A zig-zag shape of the molecules is imaged in agreement with what was observed on Ag(111) for second layer P6 molecules.[18]

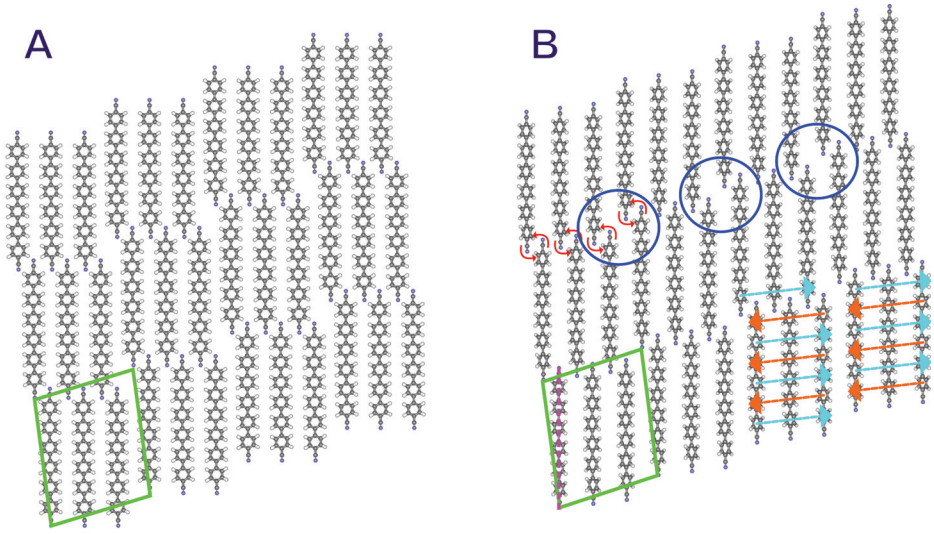

Figure 5.2: **A)** Preliminary model of the P6 self-assembly on graphene on Cu(111). **B)** Improved model of the P6 self-assembly on graphene on Cu(111) with P6 in a twisted configuration. The amount of twisting is only indicative. The unit cell is marked in green. Blue circles indicate a few of the locations where the molecules display an upward shift leading to a three-unit periodicity. Red arrows mark few of the P6 hydrogen and dipolar coupling interactions. Orange and blue dotted-arrows highlight the twisting direction of the phenyl rings.

adsorbed on graphene on metals[6,24–26] and thus, seems to be a general characteristic of these systems. However, by decoupling, the very weak or absent hybridization of the molecular states with the underlying metal is intended. Charge transfer can be present instead.[4,6,26] A peculiar feature of this self-assembly is the presence of a regular shift of one phenyl unit about every three molecules (Fig. 5.1). In principle, the observed behavior could be related to a preferential alignment of the molecules with respect to the Cu(111) or to the graphene lattice. Instead, the presence of a Moiré templating effect can be excluded by noticing that the three-unit periodicity in the P6 self-assembly is unaltered in all islands and for all samples prepared (with few exceptions showing four molecules). Considering the polycrystalline aspect of graphene on Cu(111) and the consequent variations in the Moiré periodicity, the Moiré structure cannot be the cause of the formation of this regular periodicity. A tentative model of the assembly is reported in Figure 5.2A. The unit cell

is reported in green and by analysis of the STM images we can extract the unit cell parameters that are ($a = 21 \pm 2$) Å, ($b = 26 \pm 2$) Å, with an internal angle of $82° \pm 3°$. From the model it is clear that there are many unfavorable (quadrupole) $\pi - \pi$ and steric hydrogen repulsive interactions between adjacent phenyl aromatic rings, if they would adsorb in such a flat configuration. This structure, if in gas-phase, would rearrange towards a more energetically favorable one by introducing an alternating twisting of the phenyl rings of the molecule. Looking in more detail at the STM images, one can notice that this indeed happens also for P6 on graphene. Figure 5.1C shows a high resolution image of the P6 assembly where the presence of twisted phenyl rings is clearly visible. A zig-zag shape of the molecules appears (Figure 5.1D) when scanning at a positive bias (unoccupied states). A more realistic model of the self-assembly is reported in Figure 5.2B. Herein, the tilting of the phenyl rings is qualitatively represented. Phenyls from adjacent molecules seem to interact by parallel-displaced $\pi - \pi$ interactions creating rows with phenyls twisted in the same direction. Alternating rows are thus formed. This is clearly visible from the STM images and is represented by light blue and orange arrows in the model. The P6 molecular axis is tilted (purple dotted line) by about 7° with respect to the b vector of the unit cell.

In general, π-conjugated molecules are known to interact by $\pi - \pi$ interactions with graphene[27] and thus, they can be expected to lie flat with the phenyl rings parallel to the surface. On the other hand, as described above this would lead to unfavorable inter- and intra-molecular interactions between the aromatic rings. Having the freedom of rings twisting, the P6 molecules optimize their intra- and inter-molecular interactions. This also happens on metal surfaces as discussed in previous chapters. Can something be said on the amount of ring twisting? It is difficult to determine the value for the twisting angle without performing DFT calculations. However, it is possible to make some considerations. In Chapter 3, tuning fork measurements clearly visualize the presence of twisting of the phenyl rings for P6 adsorbed on Au(111). Importantly,

this twisting is not easily revealed by STM. In the case of Ag(111), the twisting was observed by STM for P6 molecules adsorbed in the second layer while it was not visible for molecules in the first layer.[18] Surprisingly, NEXAFS measurements revealed the presence of an equal amount of twisting in both layers of about $40° - 50°$.[18] The fact that STM is sensitive to the twisting of the rings exclusively in the second layer is thus only an electronic effect caused by the weakened hybridization of the molecular orbitals with the metal. Graphene, like the first layer of molecules on a metallic surface, acts as a decoupling buffer layer and prevents strong hybridization of the molecular orbitals with the metal.

Besides parallel-displaced $\pi - \pi$ interactions, the functional cyano groups of P6 can undergo hydrogen bonding and dipolar coupling interactions. These interactions are represented in the model by the red arrows (Fig. 5.2B). Blue circles evidence the positions of the rigid shifts of the molecular arrangement that lead to the formation of a three-unit periodicity. At the center of the blue circles, the model reveals the presence of small regions of "free-space" in agreement with what is observed in the STM images (Fig. 5.1C).

In conclusion cyano dipolar coupling, hydrogen bonding and parallel-displaced $\pi - \pi$ interactions are found to determine the formation of the close-packed arrangement of P6 on graphene at sub-monolayer coverages. The intermolecular parallel-displaced $\pi - \pi$ interactions seem to be dominant driving the self-assembly to a parallel arrangement of the P6 molecules even for sub-monolayer coverage. The same parallel arrangement is observed for P6 molecules adsorbed on Ag(111) but at coverages close to 1 ML and in the second layer.[18] The molecular orbitals are imaged very clearly with STM, which indicates a weak or absent hybridization of the molecular orbitals with the substrate. A templating effect caused by the Moiré superstructure is not observed while the underling atomic lattice from the Cu(111) substrate seems to be responsible for the introduction of a periodic (three-unit) shift in the molecular arrangement. This finding shows that graphene is not a perfect decoupling layer, even

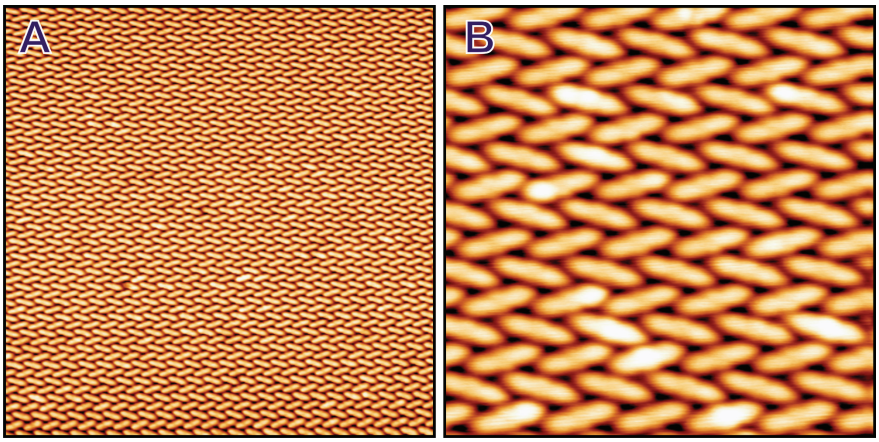

Figure 5.3: STM characterization of P3 molecules on graphene on Cu(111) at 77 K. **A)** Overview STM image (39 nm)^2, (V=−1.0 V, I=20 pA) showing an island of P3 molecules that self-assemble in a close-packed phase. The P3 molecules display a herringbone packing based on the formation of hydrogen bonds between phenyl H atoms and the N atoms of the cyano groups. **B)** Detailed STM image (9.6 nm)^2, (V=−1.6 V, I=10 pA) of the P3 packing.

for a weakly interacting system like graphene on Cu(111).

5.3 Self-assembly of cyano-functionalized terphenyl molecules on graphene on Cu(111)

Another possibility to investigate the role of the different intermolecular and molecule-substrate interactions in determining the self-assembled structures is to slightly modify the molecule and see how the assembled structure is impacted. One way is to reduce the amount of possible $\pi - \pi$ interactions by reducing the number of aromatic rings of the molecule from six to three. Thus, Leticia Monjas in the group of Anna Hirsch (RUG) synthesized terphenyldicarbonitril (P3) molecules (see Figure 5.4). We deposited P3 on graphene on Cu(111) under the same conditions as previously described for P6. Figure 5.3 shows STM images of the P3 self-assembly acquired at 77 K. The molecular orbitals are again imaged very clearly by STM, an indication that graphene pre-

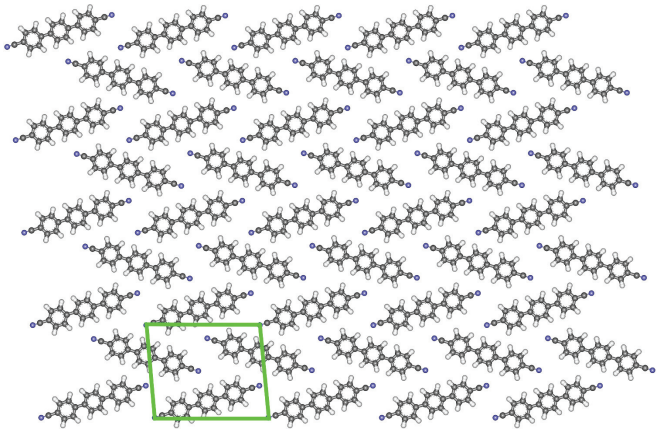

Figure 5.4: Model of the P3 self-assembly on graphene on Cu(111) assuming a planar configuration. The unit cell is reported in green.

vents hybridization of the molecular orbitals with the metallic substrate. As in the case of P6, very large islands are formed but P3 shows a different packing. As expected, by lowering the number of phenyl rings in the molecule the intermolecular $\pi - \pi$ interaction became less dominant compared to interactions of the cyano groups. P3 self-assembles in a herringbone packing in which the functional cyano groups form hydrogen bonds with the hydrogen atoms of the phenyl rings of neighboring molecules. A weak antiparallel dipolar coupling among the functional cyano groups can also be present despite the quite large distance (of 4-5 Å) between the cyano groups of neighboring molecules. A model for the self-assembled structure is reported in Figure 5.4. The unit cell is indicated in green and measures $(a = 16 \pm 1)$ Å, $(b = 13 \pm 1)$ Å, with an internal angle of $96° \pm 3°$ as extracted from STM images. The comparison between P6 and P3 self-assembly on graphene shows that parallel-displaced $\pi - \pi$ interactions are the dominant intermolecular interactions in the case of long molecules like P6 while for shorter molecules like P3 the functional cyano groups play a key role in the stabilization of the assembled structure. This is important to keep in mind if one wants to tune the functionality of organic molecules adsorbed on graphene. In the next sections the focus is on the influence of the underlying substrate

and in particular on the doping level of graphene for self-assembly and chemical reactivity of organic species on graphene.

5.4 Metal-ligand bond formation on graphene

As seen previously, linear cyano-functionalized molecules behave quite different when adsorbed on graphene in comparison to metal substrates. What about the cyano functionality: is the reactivity of these functional groups modified when adsorbed on graphene? If that is the case, can it be understood why and how this happens? In the following we will try to answer these questions. By adsorbing different metallic ad-atoms on the surface we investigated the chemical reactivity and the resulting assembly of P6 and P3 molecules on graphene on Cu(111) in conditions where metal-ligand interactions could be formed. The purpose was the formation of 2D metal-organic architectures on graphene as obtained for such functionalized molecules on various metals.

Figure 5.5 reports an overview displaying the behavior of P6 molecules on graphene when Ni, Au, Co and Fe atoms are co-adsorbed on the surface. The surface with the molecules adsorbed was exposed for about 10 seconds to a beam of metal atoms generated by an e-beam evaporator (metal rods were used except for Au where a crucible was used). The surface was kept at room temperature during deposition. Moreover, to reduce surface heating due to the thermal radiation from the e-beam evaporator, the deposition was performed by opening and closing the shutter with a period of about 2 seconds to obtain an effective exposure of 10 seconds at about 4 nA of ion current.

In contrast with Au(111), and despite the most-likely higher mobility of the P6 molecules on graphene, P6 does not show highly ordered assemblies after metal atoms deposition. The case that most resembles an ordered structure is that of cobalt, where small islands with molecules

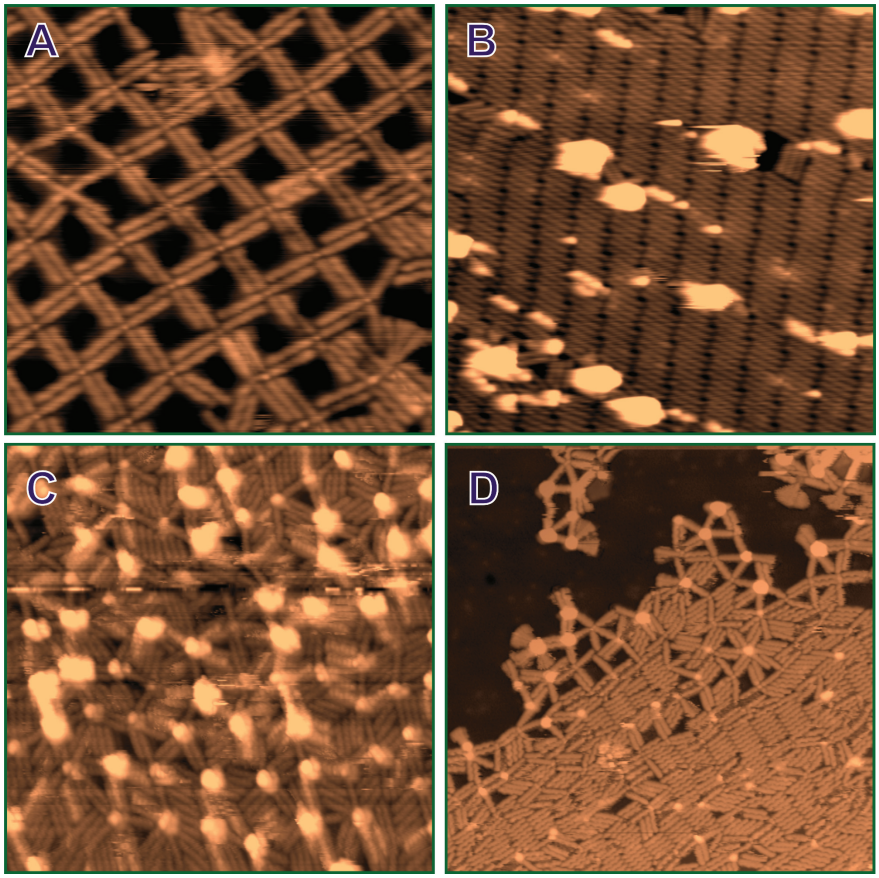

Figure 5.5: STM characterization of P6 molecules on graphene on Cu(111) at 77 K after deposition of (Co, Au, Fe, Ni) atoms. **A)** P6 with Co: STM image (24 nm)^2, (V=−0.1 V, I=20 pA) showing an island of P6 molecules that assemble in a square porous network. Formation of 4-fold molecular super-units made of four P6 molecules is observed upon addition of Co atoms. These units assemble into a network. The Co atom is imaged as a bright spot at the center of the units indicating a metal-ligand interaction. **B)** P6 with Au: STM image (36 nm)^2, (V=−1.9 V, I=20 pA) showing an island of P6 molecules perturbed by Au clusters. The addition of Au neither changes the assembly nor forms metal-coordinated bonds with P6. **C)** P6 with Fe: STM image (36 nm)^2, (V=−2.0 V, I=10 pA) showing P6 molecules interacting with Fe. Metal-coordination is present but no clear ordering. **D)** P6 with Ni: STM image (48 nm)^2, (V=−1.5 V, I=10 pA) showing P6 molecules interacting with Ni. Metal-coordination is present but no clear ordering.

displaying a square pattern could be observed. However, many defects are still present in this structure as visible in Figure 5.5A and the molecular island size is less than 100 nm. With all the other investigated metals no molecular ordering was observed, which is quite surprising considering that the same deposition conditions that produce very ordered assembled structures of P6 on metals were used. While in the case of Co, mainly 4-fold coordination is observed, Ni and Fe seem not to have clear preferences for a distinct number of coordination partners. For this reason, while Co has some potential to lead to an improved assembly through parameter optimization, Ni and Fe will never lead to a homogeneous ordering. On the other hand, Au seems to be ineffective towards the formation of metal-coordination binding motifs among cyano groups on graphene. Most of these observations contrast with the behavior of P6 molecules on Au(111).

The case of Gold:
Coordination of cyano groups with native Au atoms from the surface was suggested to explain the behavior of MK7 molecules on the Au(111) surface (see Chapter 2), leading to the formation of 3-fold coordinated units. P6 molecules on Au(111) displayed a similar 3-fold coordination (see Chapter 3). The metal coordination with Au seems to be favored by annealing while providing extra Au atoms appears not to be effective. In fact, deposition of additional Au did not show a clear enhancement of the number of coordinated centers in the case of P6 molecules on Au(111). P6 molecules that lie on graphene also show the presence of very weak or no interaction with the co-deposited Au atoms. Clusters of Au are observed while the P6 assembly is not appreciably affected by their presence. This behavior suggests that the metal-ligand interaction observed for P6 molecules with the Au(111) surface cannot be accomplished neither by single ad-atoms nor by Au atoms on graphene. The fact that annealing does not favor any metal-ligand bond for P6 on graphene (see annealing in section 5.5) and the results for 3- and 4-fold bond formation on Au(111) (presented in Chapter 3) both support this point of view.

The study of the self-assembly of cyano-functionalized molecules on a different Au surface, like *i.e.* Au(100), might be useful to obtain more insight into the subtle cyano-Au interaction.

The case of cobalt:
Deposition of Co on P6 adsorbed on Au(111) shows a well-defined ordering of the P6 molecules as reported in Chapter 3. 3-fold metal coordination develops with the cyano groups of P6 and leads to the formation of a honeycomb superlattice. Considering that the Co atoms are also interacting with the Au(111) surface, a (3+1)-fold coordination is plausible. This agrees with what is reported for the case of Ag(111).[28,29] Thus, the 4-fold coordination observed on graphene suggests that the Co atom is coordinated to 4-cyano groups leading to a 2D square planar geometry while hybridization with the substrate is weak or absent. These findings agree with previous DFT studies[29] where it was shown that 3-fold metal-coordination of functional cyano groups is energetically favored in the presence of a metallic surface, while a 4-fold binding motif is instead the energetic minimum in the gas phase. The weakened interaction with the substrate due to the presence of the graphene layer induces a change from a 3-fold to a 4-fold binding motif. This is due to the decoupling ability of graphene and the fact that graphene does not take the role of a coordination partner.

A close inspection of the assembly shows that the islands are composed of molecules that are involved in only 1 metal-ligand bond while the second cyano group remains uncoordinated. Super units comprising of four molecules are formed. The STM images show the formation of small porous networks made from the 4-fold super units that self-assembly in a square network by parallel-displaced $\pi - \pi$ interactions and hydrogen bonding. A model for this architecture is shown in Figure 5.6. The $\pi - \pi$ interactions are among phenyl rings of the P6 molecules while hydrogen bonding forms between the cyano groups and the H atoms of the phenyl groups. There is apparently no reason why only one of the two functional cyano groups should participate in the formation of metal-ligand bonds.

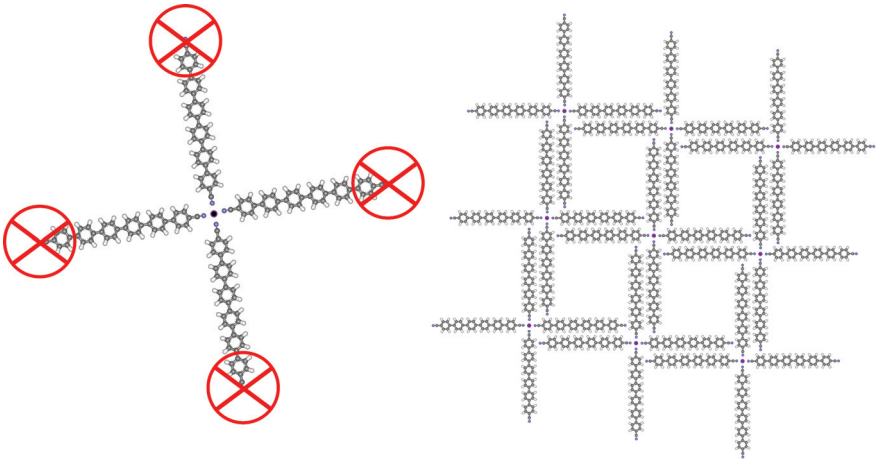

Figure 5.6: Left: Scheme showing P6 with a passivized functionality toward metal-coordination after metal-coordination with Co at the opposite side. Right: Tentative model of the 2D square network observed for P6 after deposition of Co atoms. Co-coordination, H-bonding and parallel-displaced $\pi - \pi$ interactions stabilize this architecture.

Apparently, the cyano coordination with Co atoms proceeds selectively, introducing a sort of passivation effect on the opposite cyano functional group. This behavior is sketched in Figure 5.6 and it is independent of the amount of Co deposited on the surface. In other words, the P6 molecules never coordinate with Co on both sides *i.e.* forming a fully metal-coordinated network or forming 1D chains. This is a quite unusual behavior that will be discussed later in comparison to the case of P3 molecules.

5.5 The effect of thermal annealing on the assembly structure

To form metal-coordination binding motifs, higher activation energies are often necessary with respect to the activation energies needed for the formation of H bonding and thus, annealing might help to increase the number of metal-coordinated centers. For this reason, the effect of a progressive thermal annealing (from about 100 °C to about 300 °C) for

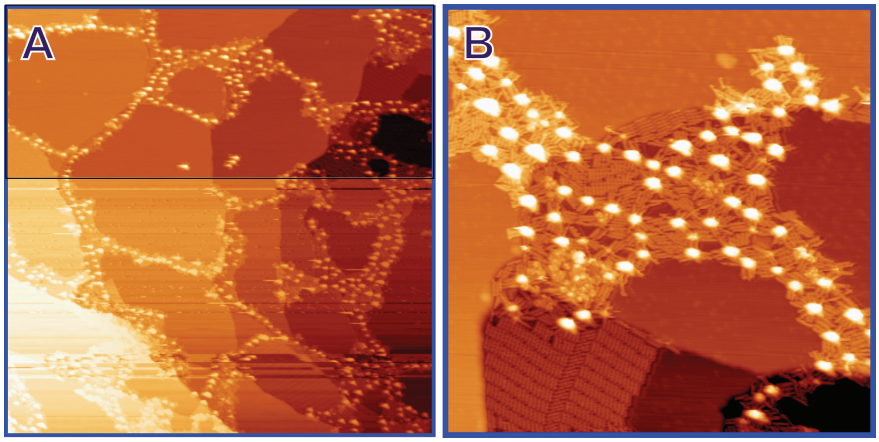

Figure 5.7: Typical behavior of the assembly of P6 molecules and metal atoms on graphene on Cu(111) after annealing at about 130 °C. The case of cobalt is reported as an example. **A)** Overview STM image (240 nm)^2, (V=−2.0 V, I=10 pA) showing cluster formation and metal migration to the grain boundaries of graphene. **B)** STM image (72 nm)^2, (V=−2.0 V, I=10 pA) showing the disruption of the 4-fold P6 super units as well as the 2D square network observed before annealing.

the systems discussed above was studied. P6 molecules were deposited on graphene at room temperature followed by metal deposition and by annealing. Figure 5.7 shows the typical effect of thermal annealing on the molecular assembly (the case of cobalt is shown). In all cases, annealing does not produce an improvement in the metal-coordinated network. Contrary, there is the tendency to recover the self-assembled molecular arrangement observed before metal deposition. It seems that the molecules prefer to rearrange in a close-packed phase. This is observed with all of the four metals studied. Large metal clusters are formed around the grain boundaries of the graphene layer where the metal atoms start to intercalate. The intercalation of metal underneath graphene with thermal annealing is a well-known fact reported in the literature.[30,31] Only a few molecules remain metal-coordinated and are located around the metal clusters at the graphene grain boundaries. The majority forms islands with a stripe structure which was discussed in the previous section. At about 300 °C the P6 molecules completely desorb from the graphene layer. Thus, annealing above room temperature does not seem to be a viable route to favor metal-coordinated molecular architectures

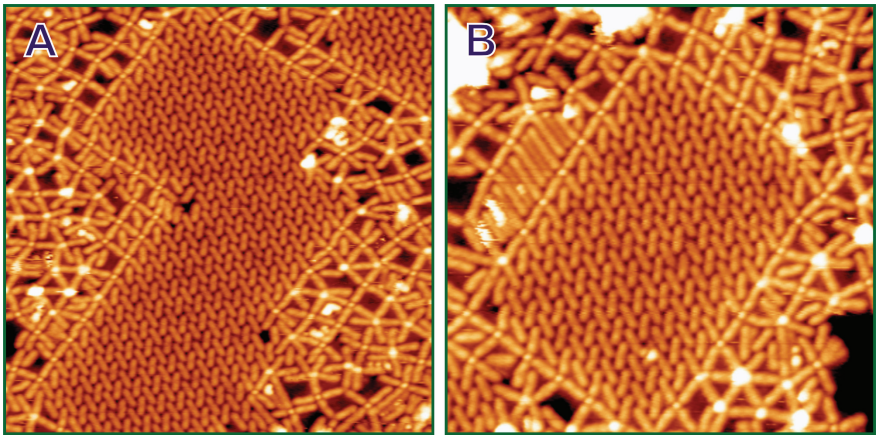

Figure 5.8: STM characterization at 77 K of a mixture of P3 and P6 molecules on graphene on Cu(111) after deposition of Co atoms. **A)** STM image (31 nm)^2, (V=−1.5 V, I=10 pA) showing an island of H-bonded P3 molecules surrounded by metal-coordinated P3 and P6 molecules. Coordinating metal atoms are imaged with a bright spot. **B)** STM image (24 nm)^2, (V=−1.5 V, I=10 pA) displaying a similar island where the different behavior of P3 and P6 is highlighted. P3 likes to form 4-fold coordination with Co on both cyano group terminations and mainly promotes 1D chains. P6(CN)-Co ligands seem instead to hinder the functionality of the opposite cyano group stopping the reaction as visible on the left. A small 2D square network of P3 is also present (top).

on graphene.

Metal-coordination of P6 and P3 molecules with Co

Deposition of Co atoms showed the most promising results toward the formation of ordered molecular architectures on graphene. For this reason, we studied the cyano-Co interaction by investigating the case of P3 molecules on graphene on Cu(111) in more detail. To compare directly the behavior of P3 and P6 a sample with both molecules mixed was prepared. Thus, Co atoms were deposited under the same conditions discussed above onto a sub-monolayer coverage of P3 mixed with P6. As visible from the STM images in Figure 5.8 the P3 molecules interact differently with Co compared to P6. In particular, the formation of 1D chains is favored. The 1D chains seem to be the starting point for the creation of a metal-coordinated 2D-network (Fig. 5.8A,B top). The 1D chains form around islands of P3 molecules that interact by hydrogen bonding. The presence of metal coordination with Co atoms is

evidenced by bright spots. As in the case of P6, the Co favor 4-fold cyano metal-coordination, but this time the passivation effect observed for P6 is absent and 1D chains can easily form. Few P6 molecules are visible in Figure 5.8B on the left, again showing the passivation effect. P3 molecules are thus more efficient than P6 in forming metal-organic structures on graphene on Cu(111). However, 2D networks are not so favored by P3 as can be seen in Figure 5.9 where STM images of a sample with only P3 molecules and Co are shown. 1D chains are marked by blue arrows and are observed much more often than 2D networks. On the contrary, in a few special regions this trend is reversed and a 2D square network is always observed. Such special regions appear as small brighter islands in the STM images. Figure 5.10 reports the high resolution STM image of one of these islands together with the model of the observed molecular architecture. Here the assembly is clearly driven towards the formation of 2D metal-coordinated networks. A remarkable difference in the STM signal for the molecules and the Co atoms is also visible. For such islands the molecular orbitals are imaged very clearly. In the STM image a sudden change is observed for the molecular contrast as soon as the molecules cross the island edge. What happens here? The explanation of this observation is connected with the results reported in Chapter 4 and is related with the modified graphene-substrate interaction in the special islands. To explain this behavior we need to recall that graphene on Cu(111) is n-doped while graphene on oxidized Cu(111) has freestanding-like properties.[32] Islands of oxide underneath the graphene layer would locally decouple the graphene from the substrate thus leading to an improved molecular decoupling. This is in agreement with the enhanced molecular orbitals resolution observed in our STM images of the molecules on top of these islands. Moreover, the darker appearance of these islands, when not covered with molecules (not shown), indicates a lower density of states near Fermi energy and thus a more insulating behavior. This observation together with the featured imaging of the molecular orbitals in these regions strongly suggests that the observed

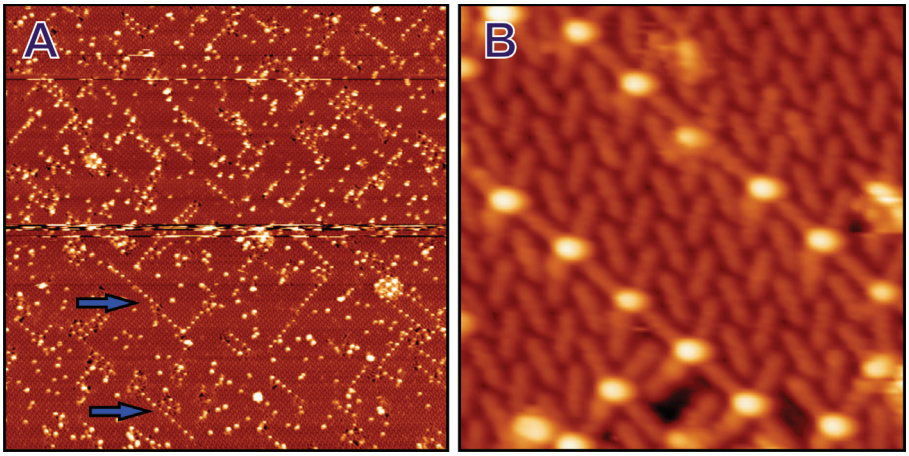

Figure 5.9: STM characterization at 77 K of sub-monolayer of P3 molecules on graphene on Cu(111) after deposition of Co atoms. **A)** STM image (120 nm)^2, (V=−1.6 V, I=10 pA) showing an island of P3 molecules after the deposition of Co. Prevalence of 1D metal-coordinated chains is observed (blue arrows). **B)** Detailed STM image (12 nm)^2, (V=−1.6 V, I=10 pA) showing the molecular arrangement and the 1D chains.

islands are indeed due to the presence of a copper oxide layer. Moreover, we know from our previous studies on graphene on Cu(111) that it is very difficult to remove all of the oxide from the copper surface prior graphene growth.

The oxide layer underneath the graphene seems to have a large effect on the reactivity of the functional cyano groups for the formation of metal-coordination binding motifs. The absence of doping of the graphene layer affects the charge transfer between graphene and the P3 molecules with a large impact on their reactivity toward metal-coordination. Experiments are planned to study the same system of P3 molecules but on graphene that is prepared on a completely oxidized Cu(111) surface. In this way, the formation of a metal-coordinated molecular network on graphene that displays a long-range ordering is expected.

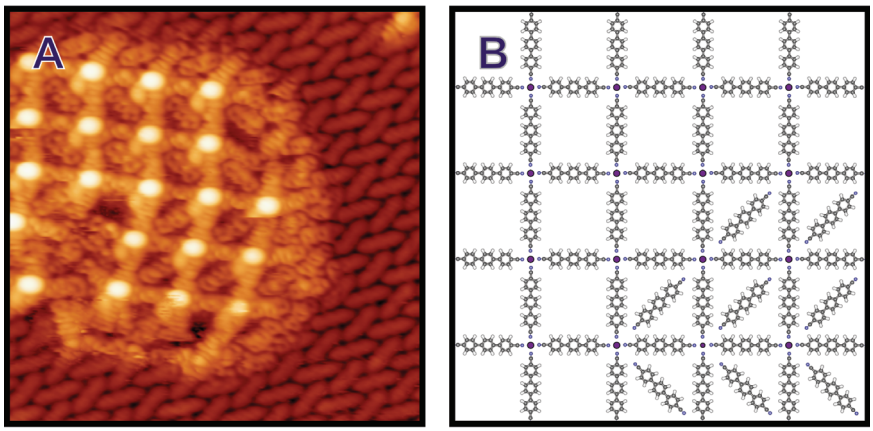

Figure 5.10: **A)** STM image $(14.5\ \text{nm})^2$, (V=−1.4 V, I=50 pA) showing the 2D Co-coordinated square network that forms in small regions where the graphene is supported by a copper oxide island. The presence of the oxide has a strong effect on the molecular assembly and the reactivity of the cyano groups. The molecular orbitals are imaged clearer inside the island than outside it. **B)** Model for the 2D Co-coordinated square network of P3 on graphene. This network differs from the network observed for P6 where the Co-coordination was not involving all the cyano groups. Some of the pores are filled with P3 molecules.

5.6 Two-dimensional porous networks on graphene stabilized by hydrogen bonding

As described in the previous sections, molecules featuring functional cyano groups do not form robust architectures on graphene and the reactivity of the cyano groups is quite sensitive to the substrate below the graphene layer. As an alternative, we decided to use non-covalent hydrogen bonding interactions for tailoring more stable and well-ordered structures.

Non-covalent hydrogen bonding is a very active interaction that drives the self-assembly and, in particular, the self-recognition of molecules on surfaces. A functional group that strongly promotes hydrogen bonding is the carboxylic group, which has the possibility to interact by double hydrogen bonding with another carboxylic group. This makes carboxylic groups useful for tuning the formation of molecular architectures. For

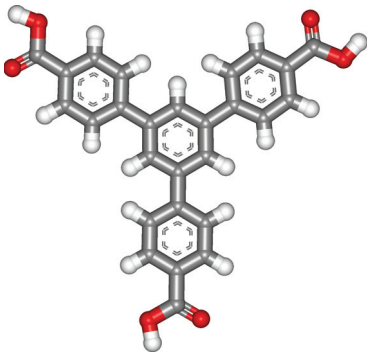

Figure 5.11: Structure of 1,3,5-Tris(4-carboxyphenyl) benzene ($C_{27}H_{18}O_6$). Carbon atoms are gray, oxygen atoms red and hydrogen atoms white, respectively.

this reason, we studied the self-assembly of 1,3,5-Tris(4-carboxyphenyl) benzene (T4) on graphene. The molecular structure of T4 is reported in Figure 5.11. The molecule has a triangular shape and features three carboxylic groups at the vertexes. In this respect, T4 is very similar to trimesic acid (TMA) that is known to favor the formation of honeycomb networks on various surfaces by hydrogen bonding.[33–35]

The T4 molecules were sublimated in UHV from a Knudsen cell evaporator onto the substrate that was kept at room temperature during deposition. The substrate used was graphene on Cu(111) that was grown according to the previously described procedure (see Chapter 4). The substrate was annealed in UHV at T=520 K prior to deposition of molecules. After deposition of $0.3 - 0.7$ ML of T4, the sample was annealed to T=400 K for 1h. The post-deposition annealing was found to improve the molecular assembly of T4 on graphene. Without an annealing step many disordered areas can be imaged by STM because the system is trapped in a kinetically-controlled metastable phase. A much improved self-assembled structure was observed after the thermal treatment. STM characterization was performed at 77 K while LEED was acquired with the sample at room temperature. The possibility to measure LEED at room temperature indicates that the double hydrogen bonding motifs and thus the T4 final self-assembled structures on graphene are stable at room temperature.

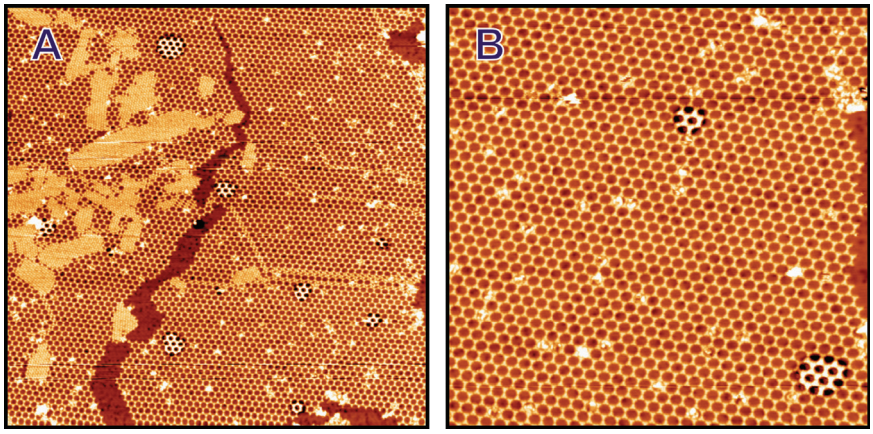

Figure 5.12: STM characterization of sub-monolayer coverage of T4 on graphene on Cu(111). A thermal annealing treatment at about 400 K for 1 h is performed to activate the self-assembly process. **A)** Overview STM image (190 nm)^2, (V=−2.3 V, I=10 pA) displaying a honeycomb supramolecular network of T4 stabilized by hydrogen bonding motifs between carboxylic groups. Defects and dislocations are present as well as few areas of close-packed arrangement of the molecules. **B)** STM image (100 nm)^2, (V=−2.3 V, I=10 pA) showing a close-up view of the porous network with few pores that are filled by other molecules. Regions displaying a darker background and brighter molecules are due to the presence of residual oxide underneath the graphene layer.

STM characterization of the self-assembled T4 network that forms on graphene after thermal annealing is reported in Figure 5.12. Large islands displaying a honeycomb network are observed. However, even after annealing, the molecular network still exhibits dislocations, defects and regions of close-packed arrangement. A better ordering of T4 on graphene is expected by performing longer annealing and slower cooling. The not optimum quality of the network observed on graphene could also be due to the presence of few residual impurities on the graphene due to the ex-situ preparation of the samples. Graphene manufactured in-situ should in principle allow the creation of higher quality molecular structures. However, we clearly saw that the annealing process that did not improve the assembly of P6 molecules on graphene is very effective in the case of T4. We attribute this different behavior to the fact that in the former case of P6, the metal-coordination binding motif has to compete with both formation of metal clusters and intercalation of metal below the graphene layer that seems to be energetically more favored.

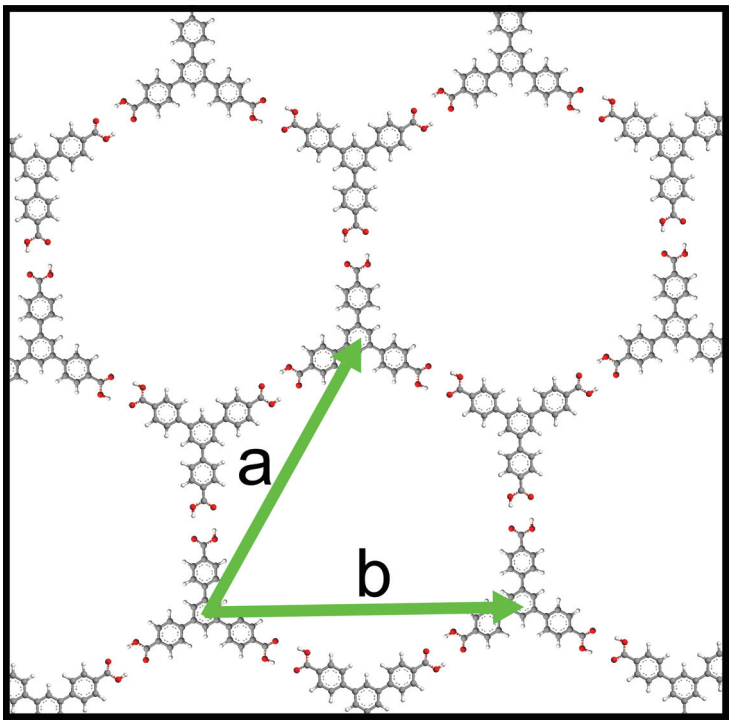

Figure 5.13: Structural model of the T4 honeycomb network formed on graphene on Cu(111). Double hydrogen bonding motifs drive the self-assembly to form a structure that is stable at room temperature. This hydrogen-bonded network seems to be robust enough to form on various different substrates. The unit cell vectors are indicated in green.

The model of the supramolecular network of T4 on graphene on Cu(111) is reported in Figure 5.13. The unit cell measures $a = b = 3.1 \pm 0.1$ nm with an internal angle of about 60°. This network is very similar to the hexagonal chicken-wire network that T4 can form on HOPG at the liquid-solid interface[36] and on Ag(111).[37] LEED measurements reported in Figure 5.14 show that the T4 network on graphene has a preferential orientation of the unit cell with respect to the underlying substrate as evidenced by the presence of stronger diffraction spots on top of a circular diffraction pattern in Figure5.14. The circular ring is due to the presence of many different rotational domains of the T4 network while the six strong spots indicate a preferential orientation with respect to the substrate main crystallographic direction. The observed align-

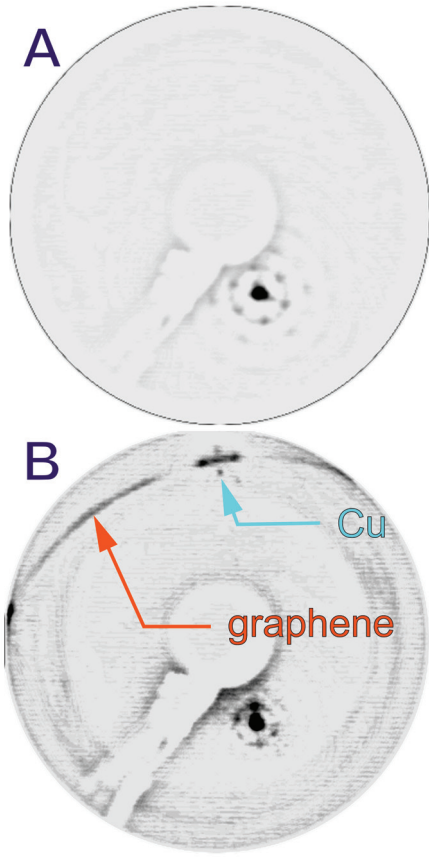

Figure 5.14: LEED measurements of the porous T4 network on graphene on Cu(111). The LEED images are processed with (gaussian difference) derivative algorithm to enhance the diffraction features. **A)** LEED pattern (E=36 eV) of the T4 network. Stronger diffraction spots are present on top of a circular background, which indicate the presence of a prevalent orientation of the T4 unit cell. **B)** LEED pattern (E=70 eV) of the T4 network where the Cu(111) and the graphene diffraction are visible. The graphene is mainly polycrystalline (circular diffraction) and the T4 unit cell is aligned along the Cu(111) main directions. However, this could also be due to a preferential alignment of the graphene as visible by the stronger signal of the graphene diffraction around the Cu(111) 1st order diffraction spots.

ment of the network's unit cell along a preferential direction is probably related to the influence of the Cu(111) substrate on the T4 molecules as was observed for P6 molecules on graphene. This corroborates the presence of a templating effect of Cu(111) that is not removed by the decoupling effect of the graphene layer. This is in agreement with what was found with the P6 molecules. Unfortunately with LEED, we cannot completely exclude that the observed templating effect could be caused by the graphene layer itself due to the fact that the graphene domains are not evenly distributed among all possible rotations but show a preferential alignment along the Cu(111) symmetry direction. This is visible in the LEED pattern (Figure 5.14B top) from the stronger signal in the

graphene diffraction near the Cu(111) spots. For this reason, it is desirable to study the T4 network on a evenly polycrystalline graphene (represented by a homogeneous circular diffraction pattern in LEED). In this way, it is possible to verify this assumption.

5.7 Quantum confinement of electrons in graphene by a H-bonded porous network

The H-bonded network formed by the self-assembly of T4 is very interesting to study the modification of the electronic properties of graphene due to patterning with a molecular superstructure. A band-gap opening is predicted due to symmetry breaking of the graphene sub-lattices[12] and might be obtained by quantum confinement of electrons in graphene. However, the latter approach has a fundamental problem.

The formation of quantized energy levels inside a potential well is a basic feature of systems governed by the Schrödinger equation. The situation is completely different in the case of electrons in graphene. Unlike normal electrons, electrons in graphene are Dirac fermions that are described by the Dirac equation for massless particles. The possibility to belong to either one or the other sub-lattice gives a pseudospin degree of freedom to the graphene electrons (see Appendix) and thus, a two-component description is needed that is very similar to the spinor wavefunctions in quantum electron dynamics (QED).[38] The pseudospin results in a chiral nature (helicity) of the electrons in graphene and has dramatic consequences for the electron tunneling processes in graphene. In fact, electrons in graphene cannot be easily confined by electrostatic potentials.[38–40] Such relativistic quasiparticles can penetrate through almost any barrier. Even in the case of high and wide barriers (*i.e.* $>$ 100 nm) the transmission coefficient is 1. This result is directly related to the so-called Klein paradox[38,41,42] and it is due to the presence of an-

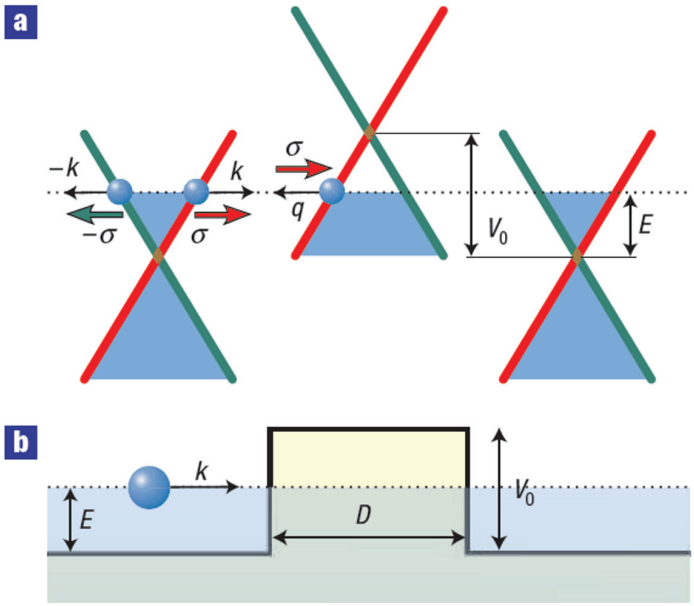

Figure 5.15: Diagram illustrating Dirac fermion scattering from a potential barrier. **a)** The dispersion near the K points is linear. Red and green lines indicate electrons in the A and B crystal sub-lattices, respectively. The pseudospin is indicated by σ. σ keeps a fixed direction along the red and green branches of the electronic spectrum. Because of pseudospin conservation, an electron traveling to the right can be scattered only to a right-moving electron or left-moving hole. **b)** Representation of the potential barrier of height V_0 and width D. The dotted line indicates the position of the Fermi energy that crosses the conduction band outside the barrier and the valence band inside it. Blue region marks the occupied electronic states. Images are taken from ref.[38]

tiparticle (hole, positron in QED) states inside the potential barriers. Hence, normal incident electrons can thus propagate through the barrier as holes. The principle of the process is reported in figure 5.15. Moreover, the potential barriers are not only ideally transparent for normal incident electrons but also for electrons impinging onto the barrier at various other angles as well as for special resonant conditions that depends on the electron momentum.[38] Thus, in general, graphene shows anti-localization effects in contrast to the Anderson localization.[40]

For the reasons discussed above, it is not possible to directly transfer the knowledge of quantum dot fabrication to the graphene case because the transmission probability of electrons in graphene through a poten-

tial barrier is almost always 1. However, the above results are under the assumption of a perfectly sharp potential well that is flat over the length-scale of the lattice constant of graphene. Thus the above results better applies to mesoscopiccally extended barriers. Moreover, the transmission coefficient can deviate from 1 for specific electron incidence angles, as well as for non-sharp onsets of the scattering potential. Thus, resonances due to electron confinement effects could be anyway expected in graphene existing inside the potential barrier as quasi-bound states due to confinement of electrons with momentum quasi-parallel to the barrier.[40,43]

5.7.1 Estimation of the size of the band-gap

In the following we try to estimate the size of the expected band-gap opening by patterning graphene with a molecular nano-porous network. A basic treatment of the *particle in a box* principle is implemented to calculate the quantum confined energy levels expected by the T4 network. Quantum confinement by nano-architectures has been studied mostly for the specific case of molecular and atomic architectures on metallic surfaces (quantum corrals)[12,44,45]. In this case the *quantum particle in a box* problem applies quite well because the surface state electrons of many metals, like Cu(111), Au(111) or Ag(111), can be treated as a 2D free-electron gas having a parabolic energy dispersion. The energy of electrons in a (parabolic) surface state can be expressed as:

$$E = \frac{p^2}{2m^*} = \frac{\hbar^2 k^2}{2m^*} \tag{5.1}$$

where $\hbar$ is the reduced Planck's constant, $k = \sqrt{k_x^2 + k_y^2}$ the electron momentum vector and m^* the effective electron mass that is characteristic of the specific metal. However, the case of graphene is different, because the electrons in graphene do not follow the standard free-electron dispersion. For our purpose, we can consider only the energy-momentum relation of electrons in graphene near the Fermi energy. Electrons close

to the Fermi energy are massless Dirac electrons that are described by a linear dispersion:

$$E = v_F \hbar k \tag{5.2}$$

where v_F is the Fermi velocity of electrons in graphene that was measured to be about $0.5 \cdot 10^6$ for graphene/Cu(111) and about $1.4 \cdot 10^6$ for graphene/oxidized Cu(111) system (see Chapter 4).

We can roughly approximate the molecules by an infinite potential well and the pores of the network to be circular. Moreover, the system is considered to be one dimensional. In this way we cannot account for states with non-zero angular momentum. A more sophisticated treatment can be done using the Bessel function.[44] Free parameters are the pore diameter and the effective electron mass in the surface state or the Fermi velocity in the case of graphene, which are all available from the experiments. For the case of T4 on graphene, the inner pore diameter measures about $d = 2.5$ nm considering the van der Waals radius of the molecules. Infinite potential wells boundary conditions give wave functions with nodes at the potential onset. With this condition the possible *quantum particle in a box* states are defined by:

$$k = \frac{2\pi}{\lambda} = \frac{\pi n}{d} \tag{5.3}$$

with n being an integer > 0. This gives an energy spectrum close to the Fermi energy approximated by

$$E = E_0 + \frac{v_F \hbar \pi n}{d} \tag{5.4}$$

where E_0 accounts for the doping energy. The calculated quantized spectrum around the Fermi energy is plotted in Figure 5.16 for the case of freestanding-like graphene as it is the case for graphene on oxidized Cu(111).

A gap of about 1.2 V results from the calculation. However, this value strongly depends on the pore size as becomes clear from the calculation

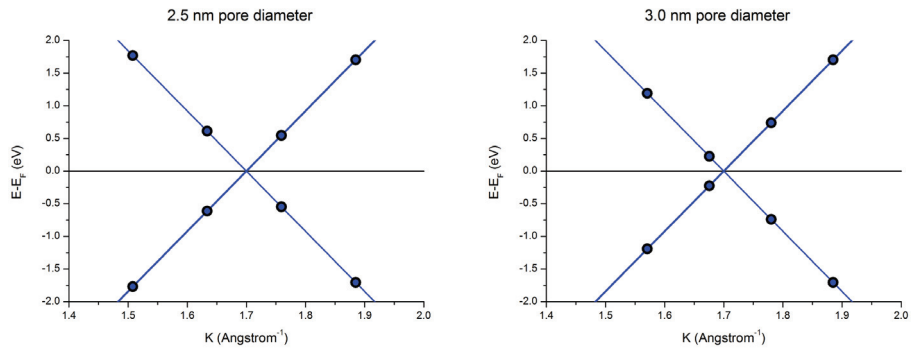

Figure 5.16: First order approximation for the quantum confined energy levels expected at the graphene Dirac points due to the presence of the T4 molecular network. Dots indicate the positions of the confined states on the π and $\pi*$ graphene bands. Left: Calculation with 2.5 nm pore inner diameter, which results in a gap opening at the Fermi energy of about 1.2 V. Right: Calculation with 3.0 nm pore inner diameter, which results in a gap opening at the Fermi energy of about 0.45 V. The gap is strongly dependent on the pore diameter and the graphene Fermi velocity.

with a slightly bigger pore (Figure 5.16 left). By this simple approximation one can already see that this system is very sensitive to the pore dimensions and geometry as well as to the graphene Fermi velocity. Moreover, quantum tunneling between adjacent pores is possible due to the non infinite potential wells of the molecular network and it is not considered in this very basic approximation. Coupling between quantum-dot like states is expected to lead to dispersive bands, as observed on metallic surfaces.[13] The dispersion renormalization would depend on the specific coupling mechanism. As a general trend, a lower value for the estimated gap can be expected due to less strict boundary conditions on the k vector of the electrons. Other effects can also be expected due to the presence of a superlattice potential,[46] anisotropic scattering[38] and the so called Zitterbewegung, or jittery motion of the wave function.[40]

5.7.2 Preliminary experimental results

Preliminary scanning tunneling spectroscopy (STS) measurements were performed to search for signs of quantum confinement effects and band opening for T4 on graphene. Unfortunately, up until now we have

not observed such effects. One possible reason is that the electrons in graphene feel the molecular superstructure as very weak scattering barriers as was also discussed above with regard to the Klein paradox. However, many studies predict measurable effects for the electronic properties of graphene due to surface modifications.[12,40,46] Another possible reason that could explain our negative preliminary results is that STS cannot discriminate univocally between electrons with different momentum. STS spectra are integrated over the "complete" Brillouin zone and are also integrated with the Cu(111) electronic bands that do not have a gap. Moreover, STS is not homogeneously sensitive to different region of the Brillouin zone, *i.e.* STM tips are in general more sensitive to electrons at the gamma point, and their sensitivity depends strongly on the tip apex. For these reasons, ARPES measurements are a better tool to study the modifications of the graphene band structure upon adsorption of T4 molecules.

To summarize: The realization of molecular self-assembled architectures on graphene was presented. Stick-like cyano-functionalized molecules (P6) showed the formation of a close-packed assembly mainly stabilized by parallel-displaced electrostatic $\pi - \pi$ interactions. Shorter P3 molecules showed a self-assembled herringbone packing where hydrogen bonding between cyano groups and phenyl H atoms was the dominant interaction. The addition of metal atoms (Au, Co, Ni, Fe) did not show a straightforward modification of the assembly towards the creation of metal-organic frameworks. Moreover, thermal annealing above room temperature is shown to deteriorate the assembly leading to the formation of metal clusters. Importantly, the chemical reactivity of the cyano functionalities toward the formation of metal-coordination bonding is found to strongly depend on the local level of graphene doping. This is a problem if one wants to realize metal-organic frameworks on graphene that lies on various substrates. Promising results in this direction are found in the case of cobalt and P3 molecules on (locally) freestanding-like graphene. However, further investigations are needed to confirm

these first results by the realization of (freestanding-like) graphene on a completely oxidized Cu(111) surface.

The realization of a molecular honeycomb network on graphene with T4 molecules featuring carboxylic groups was successfully achieved. This self-assembled network stabilized by hydrogen bonding seems more robust against differences in the amount of doping in graphene. A band-gap opening by quantum confinement of electrons in graphene by the T4 superlattice is a possibility that ask for further investigation. While preliminary results did not yet give a clear answer to this question, ARPES measurements are expected to bring more insight into this prospect.

Bibliography

[1] MacLeod, J. M. and Rosei, F. *Small* **10**(6), 1038–49 (2014).

[2] Garnica, M., Stradi, D., Barja, S., Calleja, F., Díaz, C., Alcamí, M., Martín, N., Vázquez de Parga, A. L., Martín, F., and Miranda, R. *Nature Physics* **9**(6), 368–374 (2013).

[3] Wang, Q. H. and Hersam, M. C. *Nature Chemistry* **1**(3), 206–11 (2009).

[4] Järvinen, P., Hämäläinen, S. K., Banerjee, K., Häkkinen, P., Ijäs, M., Harju, A., and Liljeroth, P. *Nano Letters* **13**(7), 3199–204 (2013).

[5] Bazarnik, M., Brede, J., Decker, R., and Wiesendanger, R. *ACS Nano* **7**(12), 11341–9 (2013).

[6] Stradi, D., Garnica, M., Díaz, C., Calleja, F., Barja, S., Martín, N., Alcamí, M., Vazquez de Parga, A. L., Miranda, R., and Martín, F. *Nanoscale* **6**(24), 15271–9 (2014).

[7] Wang, Z. F., Liu, Z., and Liu, F. *Nature Communications* **4**, 1471 (2013).

[8] Wang, Z. F., Su, N., and Liu, F. *Nano Letters* **13**(6), 2842–5 (2013).

[9] Wang, Z. F., Liu, Z., and Liu, F. *Physical Review Letters* **110**(19), 196801 (2013).

[10] Ogawa, Y., Niu, T., Wong, S. L., Tsuji, M., Wee, A. T. S., Chen, W., and Ago, H. *The Journal of Physical Chemistry C* **117**(42), 21849–21855 (2013).

[11] Li, B., Tahara, K., Adisoejoso, J., Vanderlinden, W., Mali, K. S., De Gendt, S., Tobe, Y., and De Feyter, S. *ACS Nano* **7**(12), 10764–72 (2013).

[12] Shayeganfar, F. and Rochefort, A. *Langmuir* **30**(32), 9707–16 (2014).

[13] Lobo-Checa, J., Matena, M., Müller, K., Dil, J. H., Meier, F., Gade, L. H., Jung, T. A., and Stöhr, M. *Science* **325**(5938), 300–3 (2009).

[14] Jeon, C., Hwang, H.-N., Lee, W.-G., Jung, Y. G., Kim, K. S., Park, C.-Y., and Hwang, C.-C. *Nanoscale* **5**(17), 8210–4 (2013).

[15] Batzill, M. *Surface Science Reports* **67**(3-4), 83–115 (2012).

[16] Voloshina, E. and Dedkov, Y. *Physical Chemistry Chemical Physics : PCCP* **14**(39), 13502–14 (2012).

[17] Mattevi, C., Kim, H., and Chhowalla, M. *Journal of Materials Chemistry* **21**(10), 3324 (2011).

[18] Klappenberger, F., Kühne, D., Marschall, M., Neppl, S., Krenner, W., Nefedov, A., Strunskus, T., Fink, K., Wöll, C., Klyatskaya, S., Fuhr, O., Ruben, M., and Barth, J. V. *Advanced Functional Materials* **21**(9), 1631–1642 (2011).

[19] Kühne, D., Klappenberger, F., Decker, R., Schlickum, U., Brune, H., Klyatskaya, S., Ruben, M., and Barth, J. V. *Journal of the American Chemical Society* **131**(11), 3881–3 (2009).

[20] Kühne, D., Klappenberger, F., Decker, R., Schlickum, U., Brune, H., Klyatskaya, S., Ruben, M., and Barth, J. V. *The Journal of Physical Chemistry C* **113**(41), 17851–17859 (2009).

[21] De Feyter, S. and De Schryver, F. C. *Chemical Society Reviews* **32**(3), 139–150 (2003).

[22] Yang, Y., Miao, X., Liu, G., Xu, L., Wu, T., and Deng, W. *Applied Surface Science* **263**, 73–78 (2012).

[23] Tao, F. and Bernasek, S. L. *Langmuir* **23**(7), 3513–22 (2007).

[24] Barja, S., Garnica, M., Hinarejos, J. J., Vázquez de Parga, A. L., Martín, N., and Miranda, R. *Chemical Communications* **46**(43), 8198–200 (2010).

[25] Endlich, M., Gozdzik, S., Néel, N., da Rosa, A. L., Frauenheim, T., Wehling, T. O., and Kröger, J. *The Journal of Chemical Physics* **141**(18), 184308 (2014).

[26] Uihlein, J., Peisert, H., Adler, H., Glaser, M., Polek, M., Ovsyannikov, R., and Chassé, T. *The Journal of Physical Chemistry C* **118**(19), 10106–10112 (2014).

[27] Wang, W., Zhang, Y., and Wang, Y.-B. *The Journal of Chemical Physics* **140**(9), 094302 (2014).

[28] Klyatskaya, S., Klappenberger, F., Schlickum, U., Kühne, D., Marschall, M., Reichert, J., Decker, R., Krenner, W., Zoppellaro, G., Brune, H., Barth, J. V., and Ruben, M. *Advanced Functional Materials* **21**(7), 1230–1240 (2011).

[29] Schlickum, U., Decker, R., Klappenberger, F., Zoppellaro, G., Klyatskaya, S., Ruben, M., Silanes, I., Arnau, A., Kern, K., Brune, H., and Barth, J. V. *Nano Letters* **7**(12), 3813–7 (2007).

[30] Grüneis, A. and Vyalikh, D. *Physical Review B* **77**(19), 193401 (2008).

[31] Decker, R., Brede, J., Atodiresei, N., Caciuc, V., Blügel, S., and Wiesendanger, R. *Physical Review B* **87**(4), 041403 (2013).

[32] Gottardi, S., Müller, K., Bignardi, L., Moreno-López, J. C., Pham, T. A., Ivashenko, O., Yablonskikh, M., Barinov, A., Björk, J., Rudolf, P., and Stöhr, M. *Nano Letters* **15**(2), 917–922 (2015).

[33] Griessl, S., Lackinger, M., Edelwirth, M., Hietschold, M., and Heckl, W. M. *Single Molecules* **3**(1), 25–31 (2002).

[34] Dmitriev, A., Lin, N., Weckesser, J., Barth, J. V., and Kern, K. *The Journal of Physical Chemistry B* **106**(27), 6907–6912 (2002).

[35] Lackinger, M., Griessl, S., Heckl, W. M., Hietschold, M., and Flynn, G. W. *Langmuir* **21**(11), 4984–8 (2005).

[36] Kampschulte, L., Lackinger, M., Maier, A.-K., Kishore, R. S. K., Griessl, S., Schmittel, M., and Heckl, W. M. *The Journal of Physical Chemistry B* **110**(22), 10829–10836 (2006).

[37] Ruben, M., Payer, D., Landa, A., Comisso, A., Gattinoni, C., Lin, N., Collin, J.-P., Sauvage, J.-P., De Vita, A., and Kern, K. *Journal of the American Chemical Society* **128**(49), 15644–15651 (2006).

[38] Katsnelson, M. I., Novoselov, K. S., and Geim, A. K. *Nature Physics* **2**(9), 620–625 (2006).

[39] De Martino, A., Dell'Anna, L., and Egger, R. *Physical Review Letters* **98**(6), 066802 (2007).

[40] Castro Neto, A. H., Peres, N. M. R., Novoselov, K. S., and Geim, A. K. *Reviews of Modern Physics* **81**(1), 109–162 (2009).

[41] Calogeracos, A. and Dombey, N. *Contemporary Physics* **40**(5), 313–321 (1999).

[42] Itzykson, C. and Zuber, J.-B. *Quantum field theory*. Courier Corporation, (2006).

[43] Silvestrov, P. and Efetov, K. *Physical Review Letters* **98**(1), 016802 (2007).

[44] Crommie, M. F., Lutz, C. P., and Eigler, D. M. *Science* **262**(5131), 218–20 (1993).

[45] Oka, H., Brovko, O. O., Corbetta, M., Stepanyuk, V. S., Sander, D., and Kirschner, J. *Reviews of Modern Physics* **86**, 1127–1168 (2014).

[46] Ponomarenko, L. A., Gorbachev, R. V., Yu, G. L., Elias, D. C., Jalil, R., Patel, A. A., Mishchenko, A., Mayorov, A. S., Woods, C. R., Wallbank, J. R., Mucha-Kruczynski, M., Piot, B. A., Potemski, M., Grigorieva, I. V., Novoselov, K. S., Guinea, F., Fal'ko, V. I., and Geim, A. K. *Nature* **497**(7451), 594–7 (2013).